Editors' Suggestion

Atomic Source of Single Photons in the Telecom Band

A. M. Dibos, M. Raha, C. M. Phenicie, and J. D. Thompson*
Department of Electrical Engineering, Princeton University, Princeton, New Jersey 08544, USA

(Received 31 December 2017; published 11 June 2018)

Single atoms and atomlike defects in solids are ideal quantum light sources and memories for quantum networks. However, most atomic transitions are in the ultraviolet-visible portion of the electromagnetic spectrum, where propagation losses in optical fibers are prohibitively large. Here, we observe for the first time the emission of single photons from a single Er^{3+} ion in a solid-state host, whose optical transition at 1.5 μm is in the telecom band, allowing for low-loss propagation in optical fiber. This is enabled by integrating Er^{3+} ions with silicon nanophotonic structures, which results in an enhancement of the photon emission rate by a factor of more than 650. Dozens of distinct ions can be addressed in a single device, and the splitting of the lines in a magnetic field confirms that the optical transitions are coupled to the electronic spin of the Er^{3+} ions. These results are a significant step towards long-distance quantum networks and deterministic quantum logic for photons based on a scalable silicon nanophotonics architecture.

DOI: 10.1103/PhysRevLett.120.243601

Quantum networks are a crucial ingredient for many quantum technologies, including quantum cryptography [1], modular quantum computing [2], and quantum-enhanced metrology [3]. Single atoms and atomlike defects have been used to demonstrate a variety of key tasks for quantum networks, including spin-photon entanglement [4–6], entanglement of remote atomic spins [7], and deterministic interactions between photons [8,9]. Ultimately, the long-distance distribution of entanglement is achieved by sending a photon emitted by the atom through an optical fiber. A central challenge to extending this work beyond the laboratory scale is that the losses in standard optical fibers are large for photons at the wavelength of previously studied atomic systems, ranging from approximately 8 dB/km (for NV^- color centers in diamond at 637 nm [10]) to 2 dB/km (for SiV^0 color centers in diamond [11] or InGaAs quantum dots [6], both near 980 nm). In comparison, the losses in the 1.5 μm telecom band are only 0.2 dB/km [12], which results in 10^9-fold improvement in transmission over a modest 50 km link (relative to 2 dB/km). This has motivated significant efforts to perform single-photon wavelength conversion to 1.5 μm using nonlinear optics [6,13], or to avoid fiber altogether using free-space transmission via satellites [14].

In this work, we pursue a direct solution to this challenge based on single Er^{3+} ions, which have an optical transition with a wavelength of 1.5 μm. In addition to offering lower losses in fibers, this wavelength also enables integration with technologically mature silicon nanophotonic devices [15], which we employ here. Like other rare-earth ions, Er^{3+} features coherent spin [16] and optical [17] transitions even in solid-state hosts, as the active $4f$ electrons are situated close to the nucleus and therefore only weakly coupled to phonons in the host crystal [18]. These properties have motivated the development of quantum memories for light based on rare-earth ion ensembles [19,20]. However, observations of single rare-earth ions have been hampered by the electric dipole-forbidden nature of intra-$4f$ optical transitions, which results in long excited-state lifetimes and correspondingly low photon emission rates [18]. Consequently, optical emission from single rare-earth ions (Pr^{3+} and Ce^{3+}) has only recently been observed [21–24], although single Er^{3+} ions in silicon have also been detected using a charge-sensing approach [25].

The key idea of our experimental approach is to enhance the emission rate of single Er^{3+} ions by positioning an Er-doped crystal in close proximity to a silicon photonic crystal (PC) cavity tuned to the transition frequency of the ion (Fig. 1) [26,27]. The enhancement resulting from the cavity, denoted by the Purcell factor P, is maximized for small mode-volume, low-loss cavities. Recently, other resonator geometries have been used to enhance the decay rate of rare-earth ion ensembles by a factor of 20 [27,28]. Silicon PCs capable of achieving $P > 10^5$ have been demonstrated [29,30], which would result in photon emission rates from single Er^{3+} ions of more than 10 MHz, despite the low initial rate of $2\pi \times 14$ Hz [31]. Importantly, this is possible because the Er^{3+} 1.5 μm transition is radiatively efficient despite its small transition moment, enabling large enhancement of the total emission rate by modifying the electromagnetic environment.

Our devices consist of one-dimensional silicon PCs on an Er-doped yttrium orthosilicate (Y_2SiO_5, or YSO) substrate. We fabricate the silicon PCs from a silicon-on-insulator wafer using electron beam lithography and reactive ion etching, then transfer them onto YSO using

a stamping technique. YSO is chosen as a host because it is available in high-quality, transparent single crystals, and Er substitutes easily for Y [31]. Our YSO crystals contain trace quantities of Er^{3+} with an independently measured concentration of 0.2 ppm [33]. Ions near the YSO surface couple to the cavity through the evanescent electric field, whose magnitude $|E|$ at the Si-YSO interface is 60% of its maximal value in the center of the Si layer. The substrate is mounted on a cold finger inside a closed-cycle cryostat ($T \approx 4$ K). A lensed fiber couples light to and from the single-sided cavity with around 50% one-way efficiency, and a fiber-coupled superconducting nanowire single-photon detector (SNSPD) located in a second cryostat detects light leaving the cavity [Fig. 1(c)]. We tune the frequency of the cavity resonance *in situ* by condensing gas on the surface of the device. Additional details about the fabrication and measurement techniques are discussed in the Supplemental Material [33].

We search for ions coupled to the cavity using photoluminescence excitation spectroscopy (PLE), with the pulse sequence shown in Fig. 1(d). We record a spectrum by scanning the laser frequency and cavity resonance together through a spectral region near the Er:YSO (site 1) bulk absorption resonance at 1536.46 nm. The resulting spectrum features a series of sharp peaks [Fig. 2(a)], which we interpret as the optical transitions of individual Er^{3+} ions. The width of the individual peaks is approximately 5 MHz [Fig. 2(b)]. The height of a single peak above the background saturates at high excitation powers to about 0.02 detected photons following each excitation pulse [Fig. 2(b), inset]. Given the combined detection and collection efficiency of light in the cavity (0.04), the observed count rate is consistent with a single ion with nearly perfect emission into the cavity and an incoherent excitation probability of 0.5. The inhomogeneous distribution of the individual ions' transitions results from local variations in the crystal environment caused by strain and proximity to other defects. This distribution is slightly shifted and broadened compared to the absorption spectrum of a reference bulk Er^{3+}:YSO crystal [Fig. 2(a)]; this difference could originate from strain caused by sample mounting or proximity to the surface. However, the inhomogeneous width is substantially smaller than in glass hosts such as silica fibers, which is typically of order 10 THz [18].

To quantify the strength of the atom-cavity coupling, we focus on a single peak in the inhomogeneous distribution and extract the excited-state lifetime from the time constant of the fluorescence decay [Fig. 3(a)]. The measured value, 17.0 ± 0.1 μs, is 669 ± 4 times shorter than the bulk lifetime of $1/\Gamma_0 = 11.4$ ms for Er^{3+}:YSO. To confirm that the increased decay rate results from resonant enhancement by the cavity, we tune the cavity away from the atomic transition (by an amount Δ_c) while keeping the laser frequency fixed at the atomic transition. We observe that the decay rate is described by $\Gamma = P\Gamma_0/[1 + (2\Delta_c/\kappa)^2] + \Gamma_\infty$, where $P = 658 \pm 5$ is the Purcell factor describing the cavity contribution to the enhancement, $\Gamma_\infty = (3 \pm 5)\Gamma_0$ is the asymptotic decay rate, and κ is the cavity decay rate [Fig. 3(b)]. Using the relationship $P = 4g^2/(\kappa\Gamma_0)$, we determine the complete cavity-QED parameters $(g, \kappa, \Gamma_0) = 2\pi \times (2.48$ MHz, 2.66 GHz, 14 Hz) for this ion (here, g is the single-photon Rabi frequency). The hierarchy $\kappa \gg g \gg \Gamma$ places this system in the bad-cavity or weak-coupling regime. The value of g is roughly consistent with our theoretical prediction of $2\pi \times 2.62$ MHz for an ion at the Si-YSO interface [33]; interestingly, the predicted g is similar for either electric or magnetic dipole coupling to the cavity,

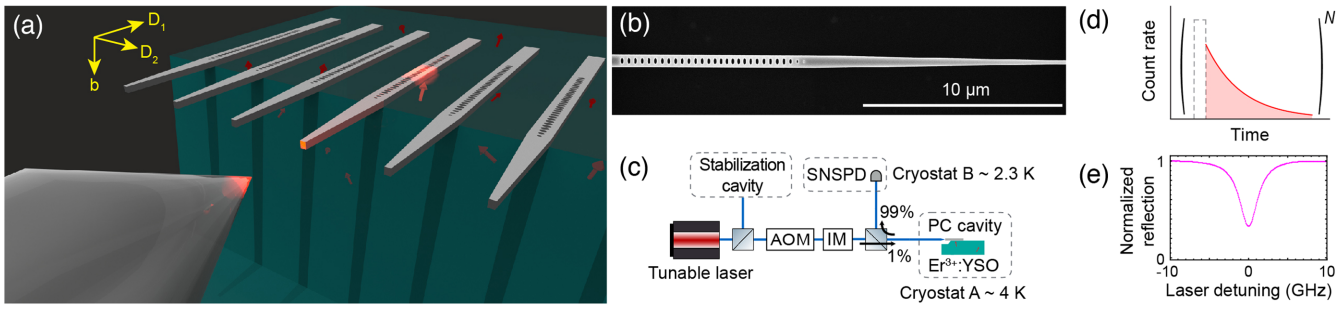

FIG. 1. Experimental configuration for enhancing Er^{3+} emission with a silicon photonic crystal. (a) Schematic illustration of the fabricated devices. Silicon waveguides patterned with photonic crystal cavities evanescently couple to Er^{3+} ion impurities in a YSO crystal. The suspended, tapered ends of the Si waveguides protrude off the edge of the YSO crystal, allowing coupling to a lensed fiber. The axes (D_1, D_2, b) denote the orientation of the YSO crystal [32]. (b) Scanning electron microscope image of a photonic crystal cavity and tapered waveguide prior to transfer onto the YSO substrate. (c) Schematic layout of the experiment. The Si-YSO device is situated in a cryostat ($T \approx 4$ K). A stabilized laser in combination with a double-pass acousto-optic modulator (AOM) and electro-optic intensity modulator (IM) produces short pulses of light with an on/off ratio of 90 dB. A superconducting nanowire single-photon detector (SNSPD) inside a second cryostat detects the return light from the cavity. (d) The PLE measurement sequence consists of a 10 μs excitation pulse, followed by a fluorescence collection window. (e) Reflection spectrum of the cavity used in these experiments, with quality factor $Q = 7.3 \times 10^4$, limited by internal losses.

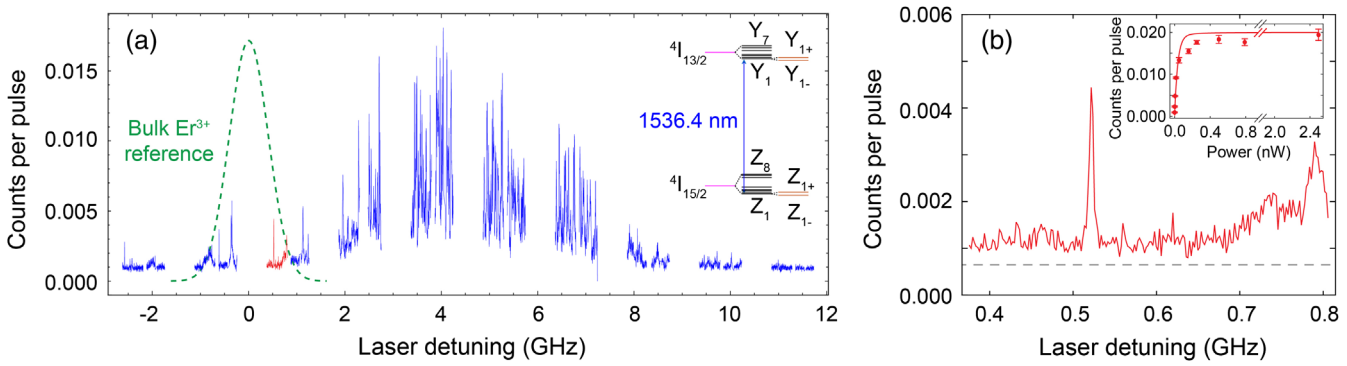

FIG. 2. Photoluminescence excitation spectrum of single ions in a dilute Er^{3+} ensemble. (a) PLE spectrum, measured by scanning the laser frequency and cavity resonance (with linewidth $\kappa = 2\pi \times 3.85$ GHz) together through a spectral region near the bulk Er:YSO absorption resonance at 1536.46 nm (determined from a second crystal, and indicated schematically by the green dashed line). The vertical axis indicates the average number of photons detected in an 82 μs integration window following each excitation pulse [as in Fig. 1(d)]. The spectrum shows individually resolvable peaks, which we interpret as the optical transitions of single Er^{3+} ions. The interruptions in the scan result from spectral regions that are inaccessible with our laser stabilization technique. Inset: Energy levels of Er^{3+} in YSO. The crystal field splits the $^{2S+1}L_J$ states of the free Er^{3+} ion (magenta lines) into $J + 1/2$ Kramers doublets (black lines), which further split into single states in a magnetic field (orange lines). The cavity is resonant with the $Z_1 - Y_1$ transition at 1536.46 nm (YSO site 1). (b) Expanded view of the red portion of (a), showing an isolated line with a width of 5 MHz (FWHM) on a nearly dark-count-limited background (gray dashed line), characteristic of the tails of the inhomogeneous distribution. Inset: The background-subtracted height of this isolated peak saturates with increasing excitation power. The solid line is a model based on independently measured parameters [33].

since the electric and magnetic dipole transition strengths are comparable in Er^{3+}:YSO [18]. The discrepancy between predicted and measured values can be attributed to the position of the ion or a misalignment between the atomic dipole moment and the local cavity polarization.

To confirm that the sharp spectral peaks result from the transitions of individual Er^{3+} ions, we measure the second-order autocorrelation function $g^{(2)}$ of the fluorescence [Fig. 3(c)]. The value of $g^{(2)}(0) = 0.055 \pm 0.007$ indicates that the majority of the detected photons originate from a single emitter. It is consistent with an estimate of accidental coincidences from dark counts [33]. The autocorrelation also shows bunching ($g^{(2)} > 1$) that decays on the order of 1 ms, which we believe results, at least in part, from spectral diffusion [33].

Lastly, we apply a magnetic field using a permanent magnet and observe that a single-ion peak splits into two lines (Fig. 4). The magnetic field is oriented along an axis at

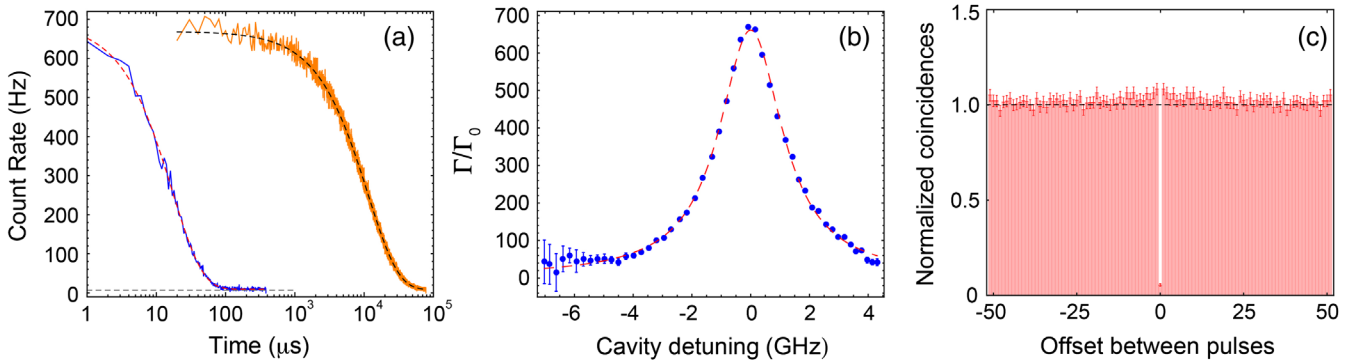

FIG. 3. Quantifying the Er^{3+}-cavity coupling, and measurement of $g^{(2)}$. (a) Time-resolved fluorescence from a single cavity-coupled Er^{3+} ion (blue) following an excitation pulse, which decays to the detector dark count rate (gray dashed line). The fluorescence from a bulk ensemble without cavity enhancement is shown for comparison (orange; measured in a second crystal, and on an arbitrary vertical scale). (b) Fixing the laser frequency to the atomic transition and sweeping the cavity resonance reveals that the decay rate enhancement Γ/Γ_0 varies with the atom-cavity detuning. A Lorentzian fit to the data (red dashed curve) yields a width of 2.62 ± 0.04 GHz (in agreement with the cavity linewidth), and a maximum decay rate enhancement of $P = 658 \pm 5$. (c) Second-order autocorrelation function ($g^{(2)}$) of the fluorescence from a single ion. We bin all photons detected after a single excitation pulse into a single time bin, so the horizontal axis shows the autocorrelation offset in units of the pulse repetition period (100 μs). The data are symmetric around zero offset since a single detector is used to record the fluorescence and compute a true autocorrelation; however, both positive and negative offsets are plotted for clarity.

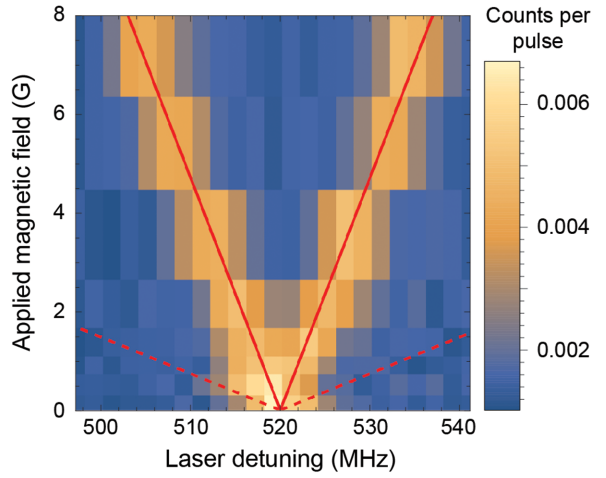

FIG. 4. Zeeman splitting of a single Er^{3+} ion spectral line. A magnetic field splits a single spectral line into two transitions. The field is oriented approximately 135 deg between the D_1 and D_2 axes in the D_1-D_2 plane. The predicted transition frequencies are shown with red lines, including an offset field of around 1 G. Since the g factors are highly anisotropic, the slope of the predicted splitting is not linear when the applied field is smaller in magnitude than the offset field, which has a different orientation.

an angle of 135 deg to the YSO D_1 axis, in the D_1-D_2 plane [Fig. 1(a)]. The measured splitting is consistent with the difference of the ground- and excited-state g factors ($\Delta g = 2.12$) for this orientation of the magnetic field [32]. The doublet nature of the ground and excited states [Fig. 2(a), inset] should give rise to four distinct transitions. However, bulk Er:YSO has been shown to have highly spin-conserving optical transitions [48], consistent with our observation of only two lines. Whether this behavior should persist in a cavity is unclear, since the branching ratio can change in a cavity with $P \gg 1$, because of polarization-dependent coupling to the cavity. Nevertheless, the brightest lines that we study likely result from ions where the stronger, spin-conserving dipole moment is aligned with the local cavity polarization, thus maintaining or even enhancing the spin-conserving nature. These measurements show that the optical transitions are coupled to the spin, which is crucial for future spin-photon entanglement.

We note that we have not been able to observe any dynamics of the ground-state spin, such as optical spin polarization. This leads us to conclude that either the optical transitions are extremely spin conserving, that the spin-lattice relaxation time (T_1) is short compared to the optical excited state lifetime, or both. Prior measurements of T_1 for Er:YSO reveal a steep temperature dependence around 4 K, with $T_1 = 1.5$ ms at 4 K, but only 7.5 μs at 6 K [49]. Therefore, a slightly elevated sample temperature resulting from poor heatsinking in the cryostat could result in a significantly reduced T_1.

The experiments described above demonstrate that nanophotonic structures can be used to enhance and efficiently collect the photon emission from Er^{3+} ions, enabling the observation of fluorescence from single Er^{3+} ions for the first time. These results suggest several avenues for further investigation. First, operating at temperatures below 1 K should increase T_1 to more than 10^3 s [33], to allow the exploration of spin-photon entanglement and coherent atom-photon interactions. While the longest spin coherence time T_2 observed for the ground state in Er:YSO is 6 μs [16] (believed to be limited by the ^{89}Y nuclear spin bath), longer spin coherence times may be achieved using fast dynamical decoupling, or by implanting Er^{3+} ions into a host crystal without nuclear spins, such as silicon [50]. Second, implanting a small number of ions into an otherwise erbium-free substrate will allow the number of ions coupled to the cavity to be controlled and eliminate background fluorescence from distant, weakly coupled ions. This may require changing to a host without yttrium, since the rare-earth elements are difficult to chemically separate from each other; several candidates are already known [18]. Finally, increasing the cavity quality factor to 10^7 [29] will increase the Purcell factor and lifetime-limited linewidth 140-fold; further improvement may be possible using smaller mode-volume cavity designs [30]. This will bring the Purcell-enhanced lifetime-limited linewidth close to the observed single-ion linewidth of 5 MHz, which is 10^3 times broader than the current lifetime-limited linewidth $2\pi \times 9$ kHz. The observed linewidth is presumably broadened by dephasing or fast spectral diffusion. Significantly lower spectral diffusion resulting in homogeneous linewidths of 74 Hz has been observed in bulk photon echo spectroscopy of Er:YSO at lower temperatures and in higher magnetic fields [17]. While the broadening mechanisms involved at low fields, as in the present work, are not well understood, future single-ion measurements will help to disentangle the contributions of phonons, ion-ion interactions, and coupling to the nuclear spin bath.

This work opens the door to realizing long-distance quantum networks based on a scalable and mature silicon nanophotonics platform. The ability to simultaneously couple the cavity to many spectrally resolvable atoms is promising for multiplexed repeater schemes, as envisioned with multimode ensemble quantum memories using rare-earth ion ensembles [19]. Indistinguishable photons from ions with different transition frequencies may be generated by frequency shifting photons during transit or using quantum eraser techniques with fast photon detection, both possible because the total inhomogeneous linewidth is less than typical electronic bandwidths. Additionally, spectral addressing of ions that are spatially nearby (the average ion-ion separation is 80 nm in the present device) is a promising starting point for exploiting their electric or magnetic dipolar interactions for quantum logic [51] or quantum simulations of strongly interacting spin systems.

We gratefully acknowledge helpful conversations with Nathalie de Leon, Andrei Faraon, Jevon Longdell. and Mikael Afzelius, as well as technical assistance from Bert Harrop. Support for this research was provided by the NSF under the EFRI ACQUIRE program (Grant No. 1640959) and the Air Force Office of Scientific Research (Grant No. FA9550-18-1-0081). C. M. P. was supported by the Department of Defense (DoD) through the National Defense Science & Engineering Graduate Fellowship (NDSEG) Program.

A. M. D, M. R., and C. M. P contributed equally to this work.

Note added in proof.—Recently, we became aware of work by T. Zhong *et al.* [52], demonstrating cavity-enhanced single-photon emission from single Nd^{3+} ions using similar techniques.

*jdthompson@princeton.edu

[1] N. Gisin, G. Ribordy, W. Tittel, and H. Zbinden, Rev. Mod. Phys. **74**, 145 (2002).
[2] C. Monroe, R. Raussendorf, A. Ruthven, K. R. Brown, P. Maunz, L. M. Duan, and J. Kim, Phys. Rev. A **89**, 022317 (2014).
[3] D. Gottesman, T. Jennewein, and S. Croke, Phys. Rev. Lett. **109**, 070503 (2012).
[4] B. B. Blinov, D. L. Moehring, L. M. Duan, and C. Monroe, Nature (London) **428**, 153 (2004).
[5] E. Togan, Y. Chu, A. S. Trifonov, L. Jiang, J. Maze, L. Childress, M. V. G. Dutt, A. S. Sorensen, P. R. Hemmer, A. S. Zibrov, and M. D. Lukin, Nature (London) **466**, 730 (2010).
[6] K. De Greve, L. Yu, P. L. McMahon, J. S. Pelc, C. M. Natarajan, N. Y. Kim, E. Abe, S. Maier, C. Schneider, M. Kamp, S. Höfling, R. H. Hadfield, A. Forchel, M. M. Fejer, and Y. Yamamoto, Nature (London) **491**, 421 (2012).
[7] C. Nölleke, A. Neuzner, A. Reiserer, C. Hahn, G. Rempe, and S. Ritter, Phys. Rev. Lett. **110**, 140403 (2013).
[8] A. Reiserer, N. Kalb, G. Rempe, and S. Ritter, Nature (London) **508**, 237 (2014).
[9] T. G. Tiecke, J. D. Thompson, N. P. de Leon, L. R. Liu, V. Vuletić, and M. D. Lukin, Nature (London) **508**, 241 (2014).
[10] H. Bernien, B. Hensen, W. Pfaff, G. Koolstra, M. S. Blok, L. Robledo, T. H. Taminiau, M. Markham, D. J. Twitchen, L. Childress, and R. Hanson, Nature (London) **497**, 86 (2013).
[11] B. C. Rose, D. Huang, Z.-H. Zhang, A. M. Tyryshkin, S. Sangtawesin, S. Srinivasan, L. Loudin, M. L. Markham, A. M. Edmonds, D. J. Twitchen, S. A. Lyon, and N. P. de Leon, arXiv:1706.01555.
[12] G. P. Agrawal, *Fiber-Optic Communications Systems*, 4th ed. (John Wiley & Sons, Inc., New York, 2011).
[13] Q. Li, M. Davanco, and K. Srinivasan, Nat. Photonics **10**, 406 (2016).
[14] J. Yin *et al.*, Science **356**, 1140 (2017).
[15] D. Thomson, A. Zilkie, J. E. Bowers, T. Komljenovic, G. T. Reed, L. Vivien, D. Marris-Morini, E. Cassan, L. Virot, J.-M. Fédéli, J.-M. Hartmann, J. H. Schmid, D.-X. Xu, F. Boeuf, P. O'Brien, G. Z. Mashanovich, and M. Nedeljkovic, J. Opt. **18**, 073003 (2016).
[16] S. Probst, H. Rotzinger, A. V. Ustinov, and P. A. Bushev, Phys. Rev. B **92**, 014421 (2015).
[17] T. Böttger, C. W. Thiel, R. L. Cone, and Y. Sun, Phys. Rev. B **79**, 115104 (2009).
[18] G. Liu and B. Jacquier, *Spectroscopic Properties of Rare Earths in Optical Materials* (Springer, New York, 2005).
[19] M. Afzelius, I. Usmani, A. Amari, B. Lauritzen, A. Walther, C. Simon, N. Sangouard, J. Minar, H. de Riedmatten, N. Gisin, and S. Kröll, Phys. Rev. Lett. **104**, 040503 (2010).
[20] M. Zhong, M. P. Hedges, R. L. Ahlefeldt, J. G. Bartholomew, S. E. Beavan, S. M. Wittig, J. J. Longdell, and M. J. Sellars, Nature (London) **517**, 177 (2015).
[21] R. Kolesov, K. Xia, R. Reuter, R. Stöhr, A. Zappe, J. Meijer, P. R. Hemmer, and J. Wrachtrup, Nat. Commun. **3**, 1029 (2012).
[22] T. Utikal, E. Eichhammer, L. Petersen, A. Renn, S. Götzinger, and V. Sandoghdar, Nat. Commun. **5**, 1 (2014).
[23] I. Nakamura, T. Yoshihiro, H. Inagawa, S. Fujiyoshi, and M. Matsushita, Sci. Rep. **4**, 542 (2014).
[24] P. Siyushev, K. Xia, R. Reuter, M. Jamali, N. Zhao, N. Yang, C. Duan, N. Kukharchyk, A. D. Wieck, R. Kolesov, and J. Wrachtrup, Nat. Commun. **5**, 773 (2014).
[25] C. Yin, M. Rancic, G. G. de Boo, N. Stavrias, J. C. McCallum, M. J. Sellars, and S. Rogge, Nature (London) **497**, 91 (2013).
[26] D. L. McAuslan, J. J. Longdell, and M. J. Sellars, Phys. Rev. A **80**, 062307 (2009).
[27] E. Miyazono, I. Craiciu, A. Arbabi, T. Zhong, and A. Faraon, Opt. Express **25**, 2863 (2017).
[28] T. Zhong, J. M. Kindem, J. G. Bartholomew, J. Rochman, I. Craiciu, E. Miyazono, M. Bettinelli, E. Cavalli, V. Verma, S. W. Nam, F. Marsili, M. D. Shaw, A. D. Beyer, and A. Faraon, Science **357**, 1392 (2017).
[29] K. Kishimoto, S. Noda, T. Asano, Y. Takahashi, and Y. Ochi, Opt. Express **25**, 1769 (2017).
[30] P. Seidler, K. Lister, U. Drechsler, J. Hofrichter, and T. Stöferle, Opt. Express **21**, 32468 (2013).
[31] T. Böttger, C. W. Thiel, Y. Sun, and R. L. Cone, Phys. Rev. B **74**, 075107 (2006).
[32] Y. Sun, T. Böttger, C. W. Thiel, and R. L. Cone, Phys. Rev. B **77**, 085124 (2008).
[33] See Supplemental Material at http://link.aps.org/supplemental/10.1103/PhysRevLett.120.243601, which includes Refs. [34–47], for additional information about device design and fabrication, as well as supplemental experimental data and analysis.
[34] J. Chan, M. Eichenfield, R. Camacho, and O. Painter, Opt. Express **17**, 3802 (2009).
[35] S. G. Johnson and J. D. Joannopoulos, Opt. Express **8**, 173 (2001).
[36] A. F. Oskooi, D. Roundy, M. Ibanescu, P. Bermel, J. D. Joannopoulos, and S. G. Johnson, Comput. Phys. Commun. **181**, 687 (2010).
[37] H. T. Dung, S. Y. Buhmann, and D.-G. Welsch, Phys. Rev. A **74**, 023803 (2006).

[38] C. Li, C. Wyon, and R. Moncorge, IEEE J. Quantum Electron. **28**, 1209 (1992).
[39] G.-H. Lee, C.-H. Lee, A. M. van der Zande, M. Han, X. Cui, G. Arefe, C. Nuckolls, T. F. Heinz, J. Hone, and P. Kim, APL Mater. **2**, 092511 (2014).
[40] S. Mosor, J. Hendrickson, B. C. Richards, J. Sweet, G. Khitrova, H. M. Gibbs, T. Yoshie, A. Scherer, O. B. Shchekin, and D. G. Deppe, Appl. Phys. Lett. **87**, 141105 (2005).
[41] S. Strauf, M. T. Rakher, I. Carmeli, K. Hennessy, C. Meier, A. Badolato, M. J. A. Dedood, P. M. Petroff, E. L. Hu, E. G. Gwinn, and D. Bouwmeester, Appl. Phys. Lett. **88**, 043116 (2006).
[42] S. Probst, H. Rotzinger, S. Wünsch, P. Jung, M. Jerger, M. Siegel, A. V. Ustinov, and P. A. Bushev, Phys. Rev. Lett. **110**, 157001 (2013).
[43] A. Abragam and B. Bleaney, *Electron Paramagnetic Resonance of Transition Ions* (Dover, New York, 1986).
[44] M. Berthel, O. Mollet, G. Dantelle, T. Gacoin, S. Huant, and A. Drezet, Phys. Rev. B **91**, 035308 (2015).
[45] M. Weber, J. Volz, K. Saucke, and H. Weinfurter, Phys. Rev. A **73**, 043406 (2006).
[46] G. Sallen, A. Tribu, T. Aichele, R. André, L. Besombes, C. Bougerol, M. Richard, S. Tatarenko, K. Kheng, and J. P. Poizat, Nat. Photonics **4**, 696 (2010).
[47] T. Böttger, Y. Sun, C. W. Thiel, and R. L. Cone, Proc. SPIE Int. Soc. Opt. Eng. **4988**, 51 (2003).
[48] S. R. Hastings-Simon, B. Lauritzen, M. U. Staudt, J. L. M. van Mechelen, C. Simon, H. de Riedmatten, M. Afzelius, and N. Gisin, Phys. Rev. B **78**, 085410 (2008).
[49] I. N. Kurkin and K. P. Chernov, Physica (Amsterdam) **101B**, 233 (1980).
[50] N. Q. Vinh, N. N. Ha, and T. Gregorkiewicz, Proc. IEEE **97**, 1269 (2009).
[51] J. J. Longdell, M. J. Sellars, and N. B. Manson, Phys. Rev. Lett. **93**, 130503 (2004).
[52] T. Zhong, J. M. Kindem, J. G. Bartholomew, J. Rochman, I. Craiciu, V. Verma, S. W. Nam, F. Marsili, M. D. Shaw, A. D. Beyer, and A. Faraon, arXiv:1803.07520.